# Lift-Curve Characteristics for an Airfoil Pitching at Constant Rate

E.J. Jumper*
*Air Force Institute of Technology, Wright-Patterson Air Force Base, Ohio*
S.J. Schreck†
*Aeronautical Systems Division, Wright-Patterson Air Force Base, Ohio*
and
R.L. Dimmick‡
*Wright-Patterson Air Force Base, Ohio*

**This paper reports the results of wind-tunnel studies of dynamic stall for an NACA 0015 airfoil pitching about the midchord at a constant rate. Time-varying pressure readings from 16 locations on the airfoil were collected and used to determine the lift, pressure-drag, and moment coefficients as functions of angle of attack for 100 test cases, covering 20 dynamic airspeed/pitch rate combinations. The dynamic-stall effects of the change (from steady flow) in the angle of attack at which separation occurs at the quarter chord and the change in the angle of attack at which stall occurs were extracted from these data and found to collapse onto a nondimensional pitch rate given by the chord times the pitch rate divided by two times the freestream velocity. The results showed that relatively slow pitch rates had dramatic effects on both the delay of stall and the magnitude of the maximum lift coefficient. The nondimensional rate is a measure of the speed of the leading edge divided by the speed of the freestream; it was found that nondimensional rates of less than 0.03 more than doubled the maximum coefficient of lift. The reduced data also clearly indicate that quarter-chord separation is systematically linked to dynamic stall.**

## Introduction

EXPERIMENTAL studies of dynamic stall have been reported in the literature since the work of Kramer[1] in 1932 and have appeared with increasing frequency until the present. References 2 and 3 are especially helpful in reviewing the experimental work that has been reported. Additionally, these references are instructive in reviewing the somewhat successful attempts at gleaning prediction methods from the experimental results. Our approach has been somewhat different; for one, we have concentrated exclusively on the problem of constant pitch rates (constant $\dot{\alpha}$), unlike the majority of experiments that studied periodic motions. More importantly, our experiments have been tailored to address specific issues that have surfaced from our concurrent theoretical studies of the constant-$\dot{\alpha}$ dynamic-stall problem. In an earlier paper,[4] the findings of an experimental study of dynamic stall for an airfoil pitching at constant rates (constant $\dot{\alpha}$) were detailed. As discussed in that paper, experimental data specifically addressing the angle of attack at which the flow separates from the upper surface of the airfoil at the quarter-chord location were needed for a comparison with a concurrent theoretical study.[5,6] Because that study was a boundary-layer analysis, the figure of merit was the angle of attack at which the flow separated at the quarter chord. Continued theoretical studies,[7,8] again addressing the constant-$\dot{\alpha}$ problem, have suggested a need for experimental information more detailed than that described in Ref. 4. These studies indicated that certain behavior might appear in the lift characteristics prior to separation (cf below). Actual stall-angle information, rather than just information about the angle at which separation occurred at the quarter chord, also seemed a natural extension of the previous experimental work.

In regard to the characteristics of the lift curve prior to separation, a separate but concurrent theoretical study used conformal mapping techniques to model the unsteady, inviscid (i.e., external) flowfield for a Joukowski airfoil pitching about the half chord at constant $\dot{\alpha}$ including the shedding of vortices into the wake.[7,8] This treatment of the flow allowed for a complete, inviscid description of the pressure distribution on the airfoil surface as a function of time. The gross effects on the lift-coefficient vs angle-of-attack curves may be summarized as follows: the modeling predicted that the airfoil should experience a sudden jump in lift coefficient at rotation onset and the lift-curve slope should be depressed (see Fig. 1).

These effects have been characterized as functions of the nondimensional $\dot{\alpha}$ given by

$$\dot{\alpha}_{ND} = \frac{\frac{1}{2}c\dot{\alpha}}{U_\infty} \tag{1}$$

where c *is* the chord, $\dot{\alpha}$ the rate of change of angle of attack, and $U_\infty$ the freestream velocity. The predicted $C_L$ jump was determined to be[7,8]

$$\Delta C_L\left(\dot{\alpha}_{ND}, \frac{t}{c}\right) = 3.14\dot{\alpha}_{ND}\left[1+\frac{2}{3}\left(\frac{t}{c}\right)\right] \tag{2}$$

where $t/c$ is the thickness ratio. The predicted effect of $\dot{\alpha}_{ND}$ on the lift-curve slope $C_{L_\alpha}$ for a zero thickness airfoil (flat plate) is shown in Fig. 2. The curve in Fig. 2 can be approx-

Presented as Paper 86-0117 at the AIAA 24th Aerospace Sciences Meeting, Reno, NV, Jan. 6-9, 1986; received Dec. 23, 1986; revision received Jan. 30, 1987. 

*Professor, Department of Aeronautics and Astronautics. Associate Fellow AIAA.

†Aeronautical Engineer (formerly, Graduate Student, Department of Aeronautics and Astronautics, Air Force Institute of Technology).

‡Aeronautical Engineer (Formerly, Graduate Student, Department of Aeronautics and Astronautics, Air Force Institute of Technology). Member AIAA.

imated by

$$C_{L_\alpha}(\dot{\alpha}_{ND}) \simeq 3.6 + 2.68 \exp(-\dot{\alpha}_{ND} \times 10^3/4.216) \quad (3)$$

Equation (3) is only slightly modified by the inclusion of thickness ratio. It is against this background that the experimental study reported on here was made.

## Experimental Approach

The collection of quarter-chord separation data as described in Ref. 4 was a relatively straightforward exercise, as was that which we will describe here; however, it should be noted that the experimental demands posed by the requirement to collect actual lift data are considerably more complex than the former. This point may be most easily demonstrated by comparing the requirements of the two experiments. In the former, only four pressure transducers were used in the vicinity of the quarter chord (see Fig. 3) and the signals were normalized, thereby relaxing the requirement on the accuracy of the measurement. In the latter, a minimum of 16 pressure transducers were needed to describe the pressure on the airfoil with sufficient detail to compute aerodynamic coefficients, with a typical time for an experiment taking on the order of ¾ s. Further, the quality of the results was directly affected by the accuracy of the pressure measurements.

The same basic setup described in Ref. 4 was used for this series of tests. A 1.02 ft chord NACA 0015 airfoil instrumented now with 16 Endevco 8507-2, 2 psi (full-range) pressure transducers at the locations indicated in Fig. 3, was again made to rotate about a rotation shaft attached at the midchord. The face diameter of the 8507-2 transducers is 0.09 in. and they were surface mounted in the airfoil. The rated frequency response of the transducers is approximately 9000 Hz (20% of the resonant frequency), far exceeding the dynamic requirements of the experiment. The airfoil assembly was mounted via the rotation shaft at approximately the center of the $5 \times 3 \times 0.25$ ft test section of the wind tunnel such that it spanned the width of the tunnel. A high-torque, constant-speed motor was attached to the rotation shaft to provide constant-$\dot{\alpha}$ pitching rates of 30–90 deg/s, depending on the voltage applied. Angular position information was provided by sensing the wiper voltage on a 10-turn potentiometer attached via a gear train to the rotation shaft.

Pressure and position data were obtained using the same microcomputer-based data acquisition system described in Ref. 4. It consisted of an S-100 bus, Z-80A-based microcomputer. Of particular interest here was the analog-to-digital (A-to-D) conversion modules. Two Dual Systems Control Corporation AIM-12 multiplexed A-to-D modules (each on an S-100 bus-compatible card) were used. These modules were software and hardware configured to sequentially read the pressure transducer output voltages in differential mode. The AIM-12 in differential mode has a 114 db common-mode rejection when configured to read ± 50 mV. The use of the Endevco transducers and Dual A-to-D board combination obviated the need for signal conditioners.

The transducers measured the pressure difference between their particular location on the airfoil surface and ambient (i.e., room) pressure. The tunnel was a draw-down type and, owing to pressure drops through the inlet screens, all pressures were biased toward negative readings, including the stagnation pressure. Under the conditions of the experiment, the maximum (absolute) voltage was approximately ⅓ full scale of the transducer design range.

The AIM-12 module can resolve to one part in 4096 (12 bit) over the full range of ± 50 mV. Combined with the pressure transducers, the resolution over the range of the experiment was such that the A-to-D conversion could resolve to approximately $1 \times 10^{-4}$ psig, so that the error introduced in a single measurement could be expected to be accurate to

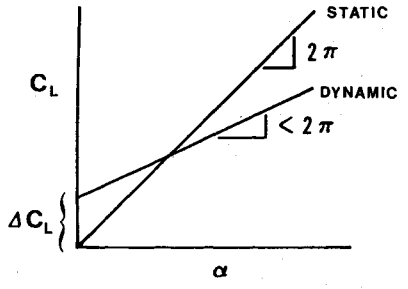


**Fig. 1 Lift-curve effects due to airfoil rotation about the midchord (from Ref. 7).**

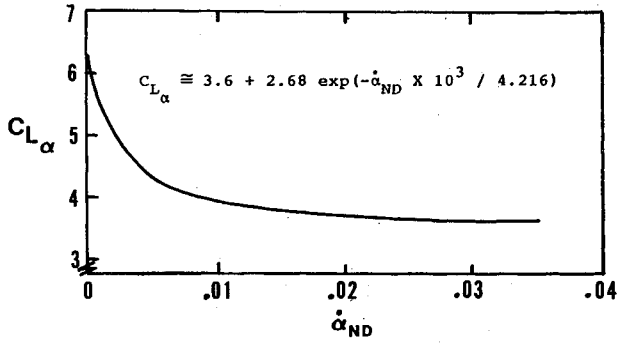


**Fig. 2 Lift-curve slope depression due to airfoil rotation about the midchord (from Ref. 7).**

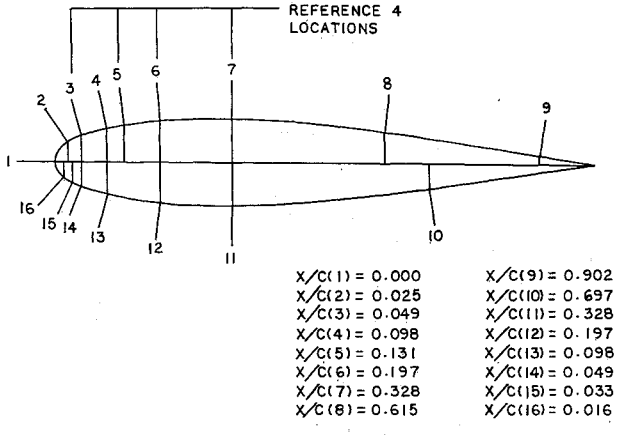


**Fig. 3 Pressure-transducer locations.**

better than 1%. These pressure measurements were then used to compute the pressure coefficients, which were then used to obtain chord-normal and chord-tangent coefficients (cf below) by computing the exact integral between polygonal curves. Thus, the error introduced by the measurement was of the linear-sum type and can be divided into error in the expected value and variance. The error in expected value in turn has two parts, the first being simple randomness error (noise) and systematic error. By looking at a steady signal and observing the error in the digital reading and comparing the individual readings with the average, the noise appeared to be random and independent from one reading to the next and from one transducer to the next. Thus, the expected value of the computed integral between polygonal lines should be that of the "exact" value. Further, an attempt was made to minimize systematic error by using our own calibration to obtain transducer sensitivities and by calibrating each transducer before and after each set of runs. The latter showed that the maximum change in sensitivity in any transducer, over the entire study, was less than 2% and there was far less change from one calibration to the next. The

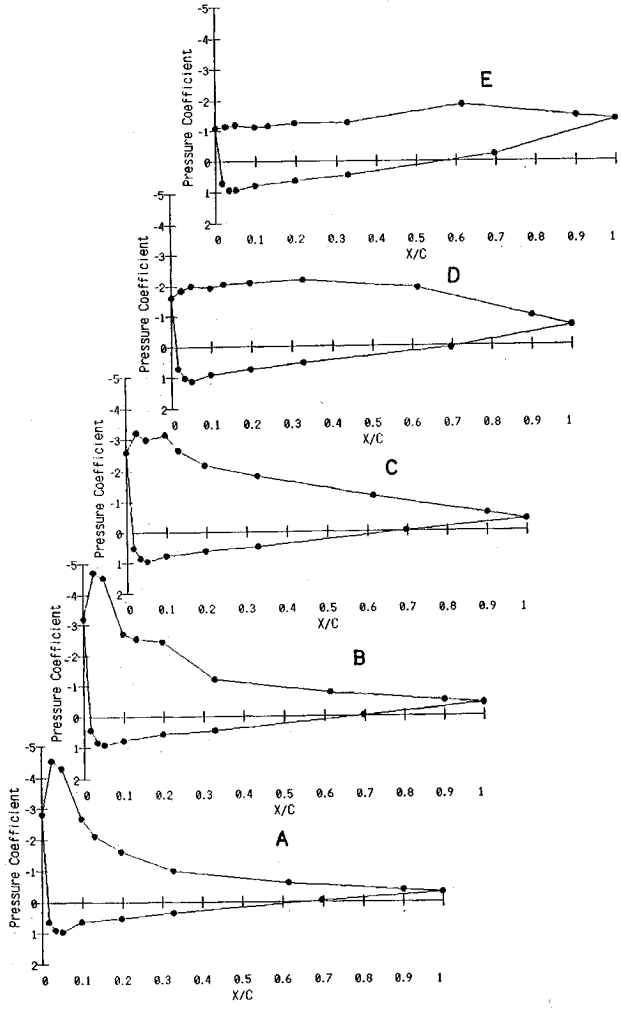


**Fig. 4 Series of $C_p$ distributions for $\dot{\alpha}_{ND} = 0.022$ case where dynamic stall was at 26.4 deg; a) $\alpha = 20.2$ deg, b) $\alpha = 22.3$ deg, c) $\alpha = 24.3$ deg, d) $\alpha = 26.4$ deg, and e) $\alpha = 29.4$ deg.**

variance can be seen to be small by examining the reduced data (cf reduced-data curves below). Finally, some error can be expected to have been introduced due to the fact that the data were collected sequentually rather than simultaneously (cf below); however, this error is clearly small for two reasons: 1) the pressure changes were small over the time between successive samples of the same transducer and 2) the changes in pressure were smooth (cf reduced-data curves below).

The data collection was accomplished by modifying the FORTRAN software of Ref. 4 to accommodate the now 16 pressure-transducer voltages as well as collecting the position voltage and internal time-clock hacks. The sample rate was made to be 4250 samples/s by using no time-loop delays in the data collection program. The readings were stored in memory and then written to disk at the completion of an experiment. The same microcomputer system was then used to reduce the data into the various appropriate forms needed to interpret the results. For more details, see Refs. 9 and 10.

## Results

A total of 100 dynamic-stall data runs were made at 5 tunnel speeds with flow velocities of 26–48 ft/s (Reynolds number range, $1.58\text{–}2.81 \times 10^5$). At each tunnel speed, four pitch rates were used and each velocity/pitch-rate combination was repeated five times. Each dynamic run was started at approximately 0 deg angle of attack. Additionally, a static $C_L$ vs $\alpha$ run was made at each tunnel speed of interest.

Since a time signal, a location signal, and 16 pressure signals were sampled in a serial fashion, a picture of the pressure distribution at a particular instant in time was approximated by linearly interpolating the signals closest to the time of interest. This yielded consistent pressure distributions from one run to the next of the duplicated runs. Examples of the results of a dynamic data run for $\dot{\alpha}_{ND} = 0.022$ are given in Fig. 4, representing distributions ranging from prior to stall to beyond dynamic stall. It should be noted that the point at $(x/c) = 1.0$ was estimated following McAlister et al.,[11] using the readings from transducers 8 and 9 (cf Fig. 3). The chord-normal aerodynamic coefficient $C_Y$ was obtained by numerical integration that found the area between

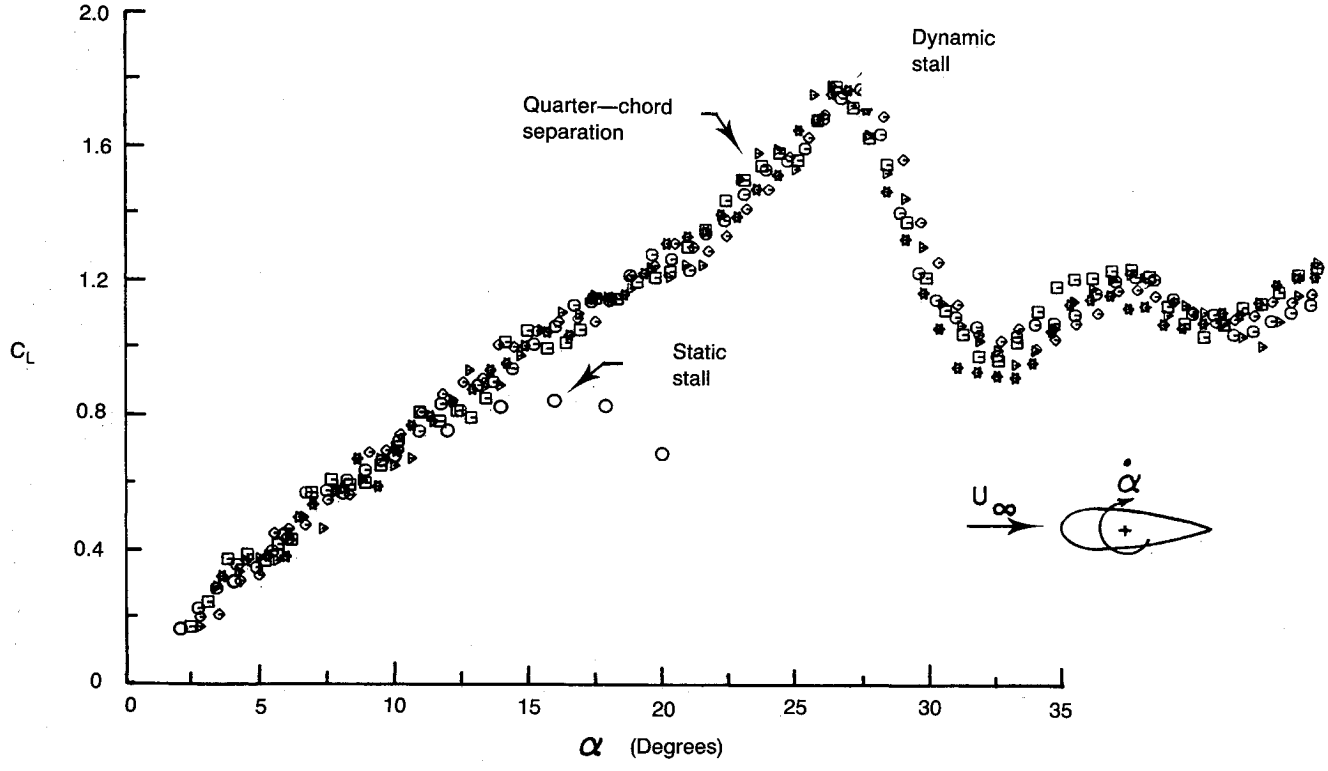


**Fig. 5 Lift curve for $\dot{\alpha}_{ND} = 0.020$, $\dot{\alpha} = 68.39$ deg/s, $U_\infty = 30.12$ ft/s.**

polygonal curves of the pressure coefficients of the type shown in Fig. 4 as follows:

$$C_Y = -\oint C_P \mathrm{d}\left(\frac{x}{c}\right) \tag{4}$$

where $C_p$ is the pressure coefficient and $(x/c)$ the ratio of the distance from the leading edge divided by the chord. In a similar way, the chord-tangent aerodynamic coefficient $C_X$ was numerically determined by integrating with respect to $(y/c)$. The lift coefficient and pressure-drag coefficient were then determined by

$$C_L = C_Y \cos\alpha - C_X \sin\alpha \tag{5}$$

and

$$C_D = C_Y \sin\alpha + C_X \cos\alpha \tag{6}$$

Finally, the quarter-chord moment coefficient was found by numerical integration of

$$(C_M)_{1/4c} = \oint C_p\left(\frac{x}{c} - 0.25\right)\mathrm{d}\left(\frac{x}{c}\right) \tag{7}$$

For more details, see Refs. 9 and 10.

The results of these reduced data are summarized in Figs. 5, 6, 8, 9, 11, and 12. These figures include $C_L$ vs $\alpha$, $C_D$ vs $\alpha$, and $C_M$ vs $\alpha$, in various formats (for more extensive data sets, see Ref. 12).

## Discussion

### Lift-Curve Characteristics

Figure 5 presents data from one dynamic combination of tunnel velocity and constant $\dot{\alpha}$, such that $\dot{\alpha}_{ND} = 0.02$ ($U_\infty = 30.12$ ft/s, $\dot{\alpha} = 68.4$ deg/s). The data represent five duplicated runs. A number of general comments may be made. First, the reproducibility of the data is worthy of comment. Each data point represents an integration over the 16 pressure coefficients obtained via the pressure transducers. Further, the data of Fig. 5 represent every possible reduced data point (up to the $\alpha$ shown; but data beyond the cutoff $\alpha$ of the graph do exist, cf below); that is to say, no data point has been selectively removed. Thus, we may say that not only did a single run have a small data scatter (i.e., variance), but there is little scatter from one run to the next for the same dynamic case. The data are, then, highly repeatable. Further, this reproducibility extends beyond the dynamic-stall location (see Fig. 5) into the periodic region beyond stall.

As discussed in Ref. 4, it is also possible to extract the separation at quarter-chord angle of attack from the pressure-transducer information. This point is located by the arrow labeled "quarter-chord separation" in Fig. 5. It may be noted that somewhat to the left of this point (i.e., lower $\alpha$) the lift curve flattens (plateaus) before continuing to rise; this feature is present to this or a lesser degree in all the dynamic runs. Smoke-visualization movies of constant-$\dot{\alpha}$, NACA-0012-airfoil experiments by Walker et al.[13] show that separation begins at the trailing edge and moves forward as $\alpha$ increases. In all cases, although the flow is separated, the general flow pattern is along the upper surface of the airfoil up to at least the point where the separation has progressed forward to the quarter-chord point. As the separation moves forward of the quarter-chord, the flow catastrophically detaches from the airfoil and forms a large, energetic vortex over the forward portion of the airfoil. This vortex is subsequently convected downstream over the airfoil. At lower $\dot{\alpha}_{ND}$, this catastrophic detachment of the flow appears to be almost coincident with separation arrival at the quarter-chord (within a movie frame). At higher $\dot{\alpha}_{ND}$, however, this event is noticeably delayed (up to several movie frames) and may not occur until the separation has progressed to nearly the leading edge.

From this detachment point to the dynamic-stall point, the lift curve is shaped similar to that predicted analytically by Chow and Chiu[14] for a vortex convecting over an airfoil. A convected-vortex explanation for this portion of the lift curve is also consistent with the visual information of Walker et al.[13]

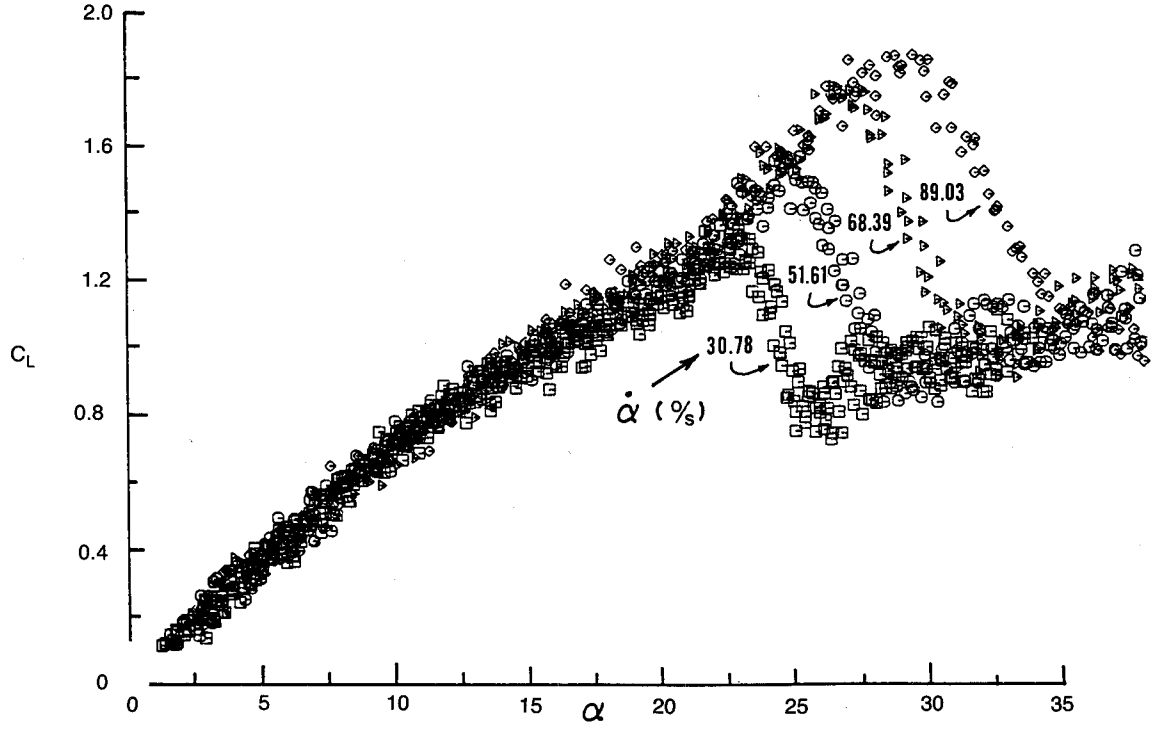


**Fig. 6 Overlay of four data sets at a tunnel speed of approximately 30 ft/s and angular rates of 30.78, 51.61, 68.39, and 89.03 deg/s, respectively.**

Finally, comment should be made about the extent of the dynamic-lift augmentation. To underscore this, the reader should be reminded that Fig. 5 is for an $\dot{\alpha}_{ND}$ of 0.02. Referring to Eq. (1), it can be seen that $\dot{\alpha}_{ND}$ is the ratio of the leading-edge speed (i.e., $\frac{1}{2}c\dot{\alpha}$) to the magnitude of the freestream velocity for the case of an airfoil pitching about the midchord. As such, the leading-edge speed is only 2% of the freestream velocity, a mere perturbation. Yet the $(C_L)_{MAX}$ has more than doubled, going from approximately 0.8 in the static case to nearly 2.0 in the dynamic case.

Figure 6 shows the effect of increasing $\dot{\alpha}$ for the same freestream velocity. The data of Fig. 5 are second from the uppermost curve. Similar curves may be overlaid for each of the five wind-tunnel speeds; the reader is directed to Ref. 12 for additional curves. Referring again to Fig. 5, the change from static conditions in both the angle at which the flow separates at the quarter-chord and the angle of stall may be determined for each of the 20 $\dot{\alpha} - U_\infty$ dynamic runs and collapsed onto $\dot{\alpha}_{ND}$. The result of this exercise is given in Fig. 7. The cross-hatched region contains both the present results as well as those from Ref. 4 and is shown to be consistent with the previous results. The change in dynamic-stall angle of attack is seen to diverge from the change in quarter-chord separation angle of attack with increasing $\dot{\alpha}_{ND}$.

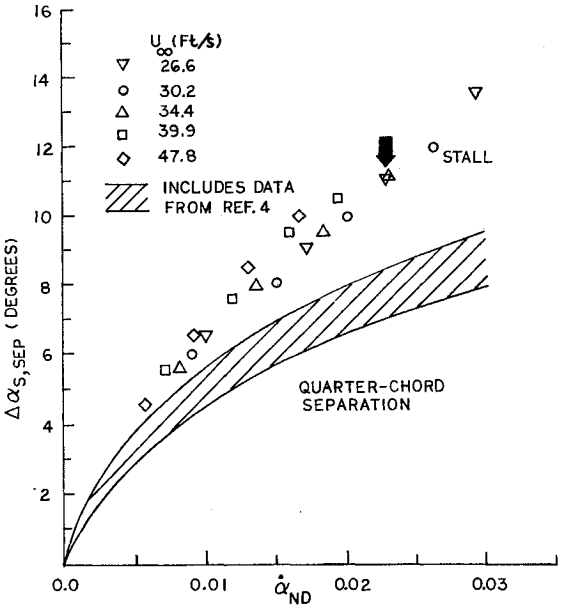


**Fig. 7 Dynamic change (from steady flow) in angle of attack for stall $\Delta\alpha_S$ and quarter-chord separation $\Delta\alpha_{SEP}$ as functions of $\dot{\alpha}_{ND}$; arrow indicates two data sets detailed further in Figs. 8, 11, and 12.**

Referring to the earlier arguments concerning separation, it is possible to demonstrate that this divergence is consistent with the convection of the vortex over the airfoil. First, let us assume that the catastrophic detachment of the flow and formation of the vortex is coincident with quarter-chord separation (although, as discussed above, this is not absolutely true—there is only a very short delay between the events even in the most exaggerated experimental cases). Once the vortex has detached, it becomes a free vortex subject to motion based on the flow velocity. If we assume that its convection speed is approximately $U_\infty$ and, following Chow and Chiu,[14] the vortex influences the lift spike over a distance of roughly the chord length $c$, then the convection time of this influence is

$$t_c \simeq k\frac{\frac{1}{2}c}{U_\infty} \tag{8}$$

where $k$ is a constant of proportionality, the $\frac{1}{2}$ being introduced for convenience. In this time, the angle of attack will change by

$$\Delta\alpha = \dot{\alpha}t_c \simeq k\left(\frac{\frac{1}{2}c\dot{\alpha}}{U_\infty}\right) \tag{9}$$

so that the difference between the separation angle of attack and the stall angle of attack should scale as

$$\Delta\alpha_s - \Delta\alpha_{SEP} \simeq k\dot{\alpha}_{ND} \tag{10}$$

Thus, such a treatment would indicate that the difference between the two should widen, approximately linearly, with increasing $\dot{\alpha}_{ND}$. Inspection of Fig. 7 demonstrates that the data appear to be consistent with these notions.

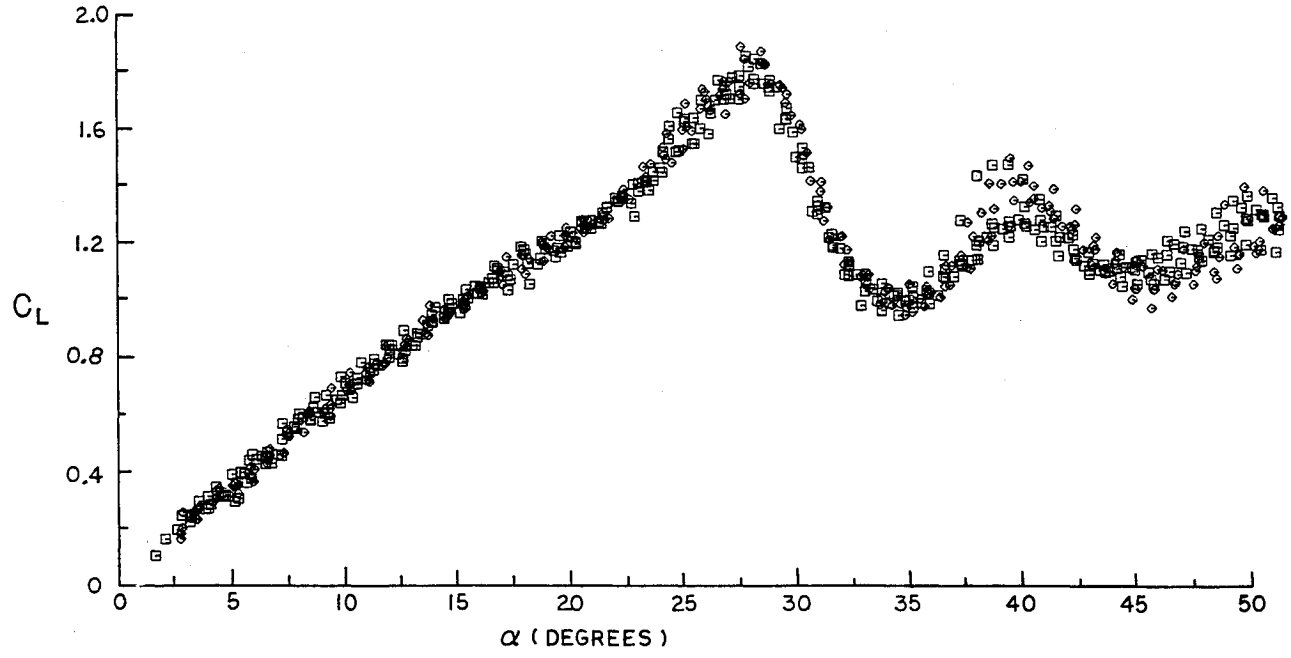


**Fig. 8 Overlay of lift curves for data sets indicated by the arrow in Fig. 7 ($\dot{\alpha}_{ND} \simeq 0.023$).**

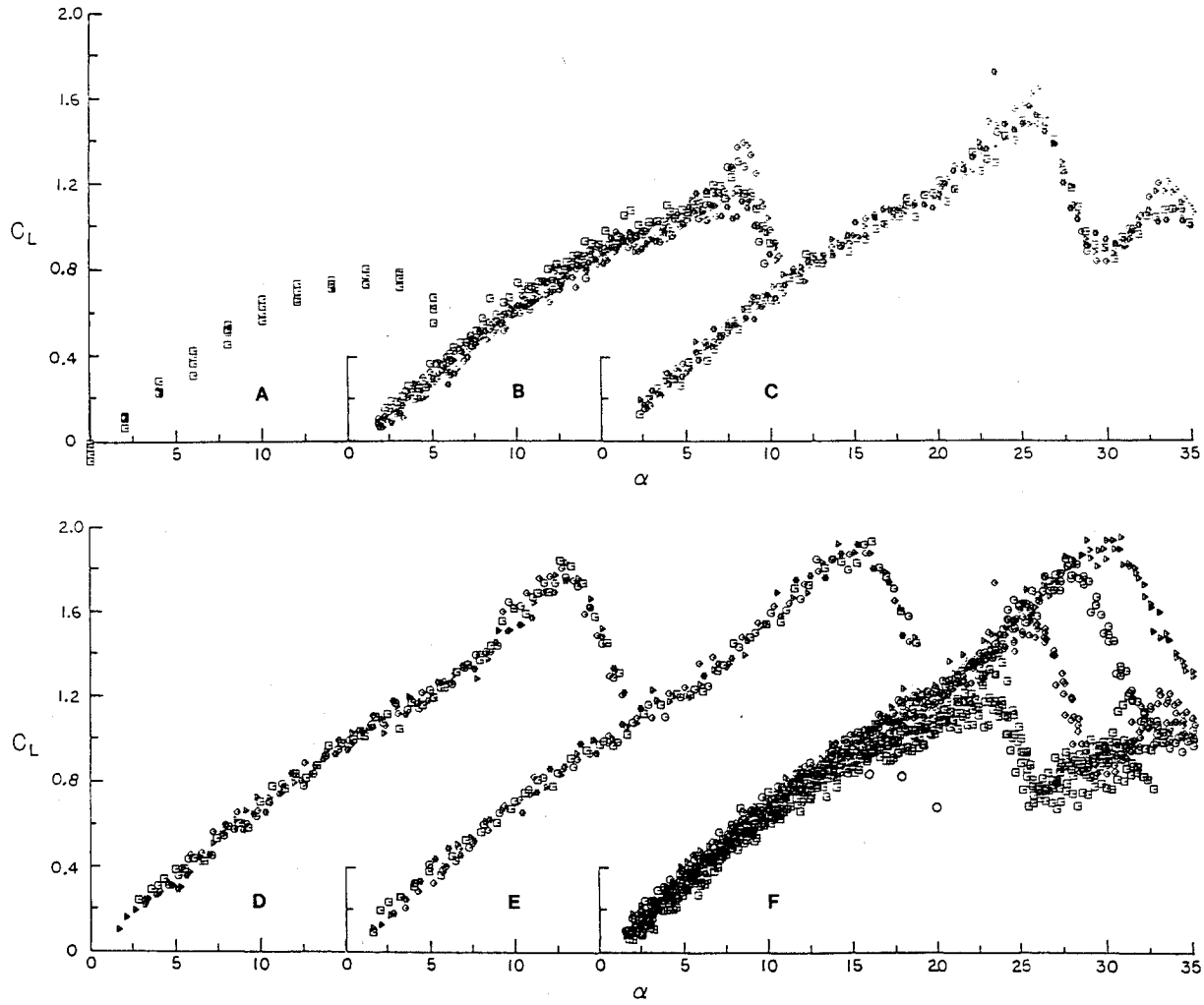


**Fig. 9 Complete series of runs at 26.6 ft/s, including an overlay of the static curve and all four dynamic cases: a) static, b) $\dot{\alpha}=29.34$ deg/s, c) $\dot{\alpha}=52.16$ deg/s, d) $\dot{\alpha}=69.49$ deg/s, e) $\dot{\alpha}=87.15$ deg/s, and f) overlay.**

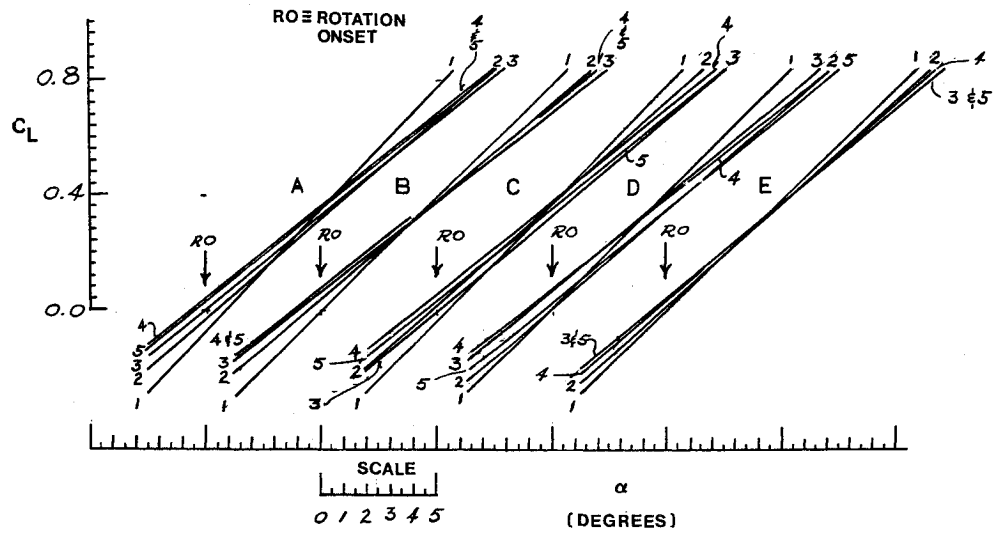


**Fig. 10 Straight-line fit of linear portion of lift curves for five tunnel speeds. Increasing numbers indicate increasing $\alpha$ at a given tunnel speed, 1 being the static slope: a) 26.6 ft/s, b) 30.2 ft/s, c)34.4 ft/s, d) 39.9 ft/s, and e) 47.8ft/s.**

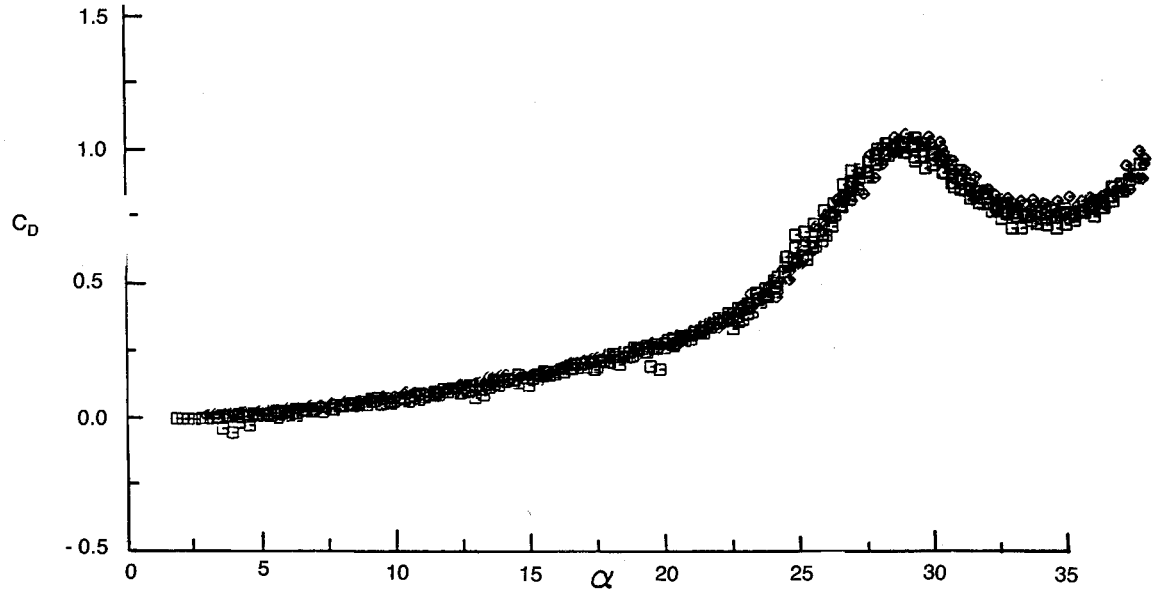


**Fig. 11 Overlay of pressure-drag coefficient vs angle-of-attack curves for the two data sets indicated by the arrow in Fig. 7 ($\dot{\alpha}_{ND} \simeq 0.023$).**

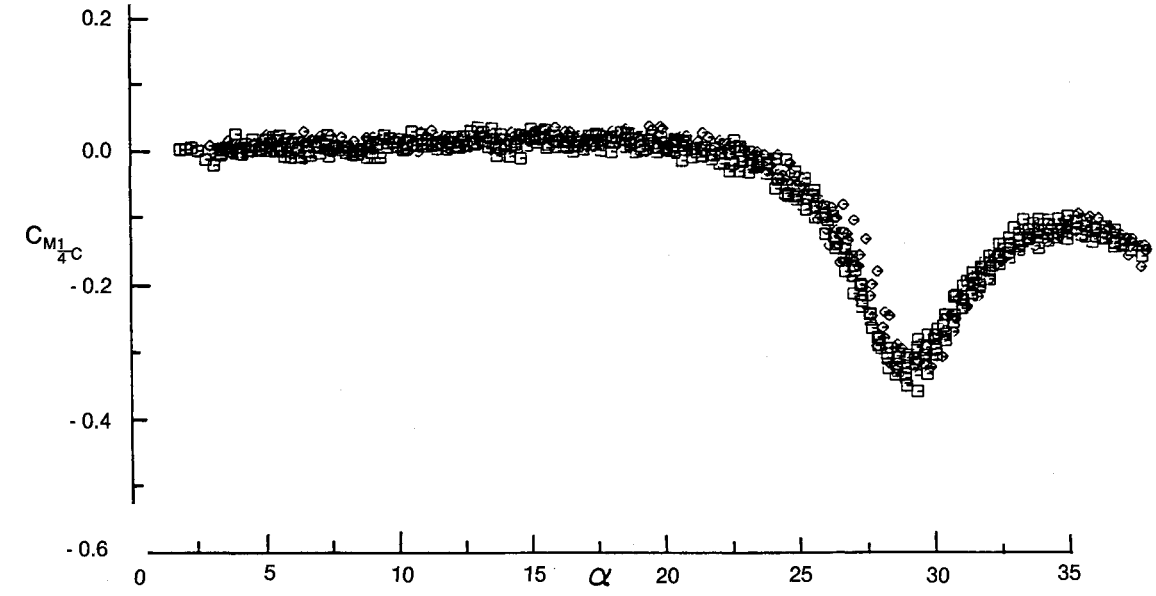


**Fig. 12 Overlay of quarter-chord moment coefficient vs angle-of-attack curves for the two data sets indicated by the arrow in Fig. 7 ($\dot{\alpha}_{ND} \simeq 0.023$).**

We now return to the question of reproducibility. We have already mentioned the reproducibility of the data for a single $\dot{\alpha} - U_\infty$ dynamic combination; we now direct the reader's attention to the two arrow-indicated data points on Fig. 7. Note that the two data points are for different $U_\infty$, one for 26.6 ft/s and one for 34.4 ft/s; however, their $\dot{\alpha}$ are such that they have nearly identical $\dot{\alpha}_{ND}$ ($\sim 0.023$). Figure 8 is an overlay of these two separate dynamic cases. We note that the scatter up to and beyond stall is as slight as it is for duplicated runs of a single dynamic $\dot{\alpha} - U_\infty$ combination (cf Fig. 5). Further, the detail in the plateauing appears to be both preserved and duplicated for an $\dot{\alpha}_{ND}$ family. This similarity is preserved even far into the poststall region, as can be seen in Fig. 8. Again, we believe that the reason for this is similar to that leading to the development of Eqs. (8–10).

**Preseparation Characteristics**

As mentioned in the Introduction, a concurrent study indicated that there may be some subtle characteristics in the lift curves during the time that the flow is "completely attached" to the airfoil (see Figs. 1 and 2). Figure 9 shows the complete series of runs at 26.6 ft/s including the final overlay of these data. If just the overlay is examined, one might suspect that the behavior suggested in Figs. 1 and 2 is either masked in data scatter or not present in the data. However, if each curve is fitted with a straight line only in the linear portion of the curve (i.e., low $\alpha$), a pattern does seem to be present. This is what has been done in Fig. 10.

Each group of lines in Fig. 10 represents a set of runs at a given tunnel velocity. The numbers indicate increasing $\dot{\alpha}$, 1 being the static lift-curve slope. The curve on the extreme left is for the curves of Fig. 9. Indeed, the trends suggested

by Eqs. (2) and (3) do appear to be present at approximately the magnitudes suggested by the concurrent study. This suggestion, however, is not definitive, as can be seen by a few cases of inversions in the trends of the reduced curves. A general agreement, however, does appear to be present and one can point to a number of possible contributors to the few discrepancies, such as the possibility that the runs may not have started at exactly $\alpha$ equal to 0 deg, etc. Without doing this, we are satisfied to simply point out the suggestion that the subtleties predicted by Refs. 7 and 8 may well exist.

#### Drag and Moment Characteristics

Because of the reproducibility of the $C_L$ vs $\alpha$ data, both for a single $\dot{\alpha}-U_\infty$ combination, as well as for an $\dot{\alpha}_{ND}$ family, it would be expected that the $C_D$ and $C_M$ data would show similar reproducibility, and such is the case. Figures 11 and 12 show typical sets of data for $\dot{\alpha}_{ND}$ family ($\dot{\alpha}_{ND} \simeq 0.023$) and is representative of all the runs. It should be noted that the $C_D$ curve is pressure drag only. Although any number of things might be discussed with regard to these data, we will be satisfied here to mention only three points: 1) the drag does not begin its sharp rise until separation reaches the quarter chord (this is consistent with the comment above concerning flow detachment); 2) the moment buildup is also coincident with drag rise and is a pitch-down moment; and 3) the moment coefficient at the quarter chord does not seem to be affected by the rotation in the sense that it is essentially zero prior to flow detachment.

#### General Comments

It should be noted that Francis et al.[15] and Walker et al.[16] also investigated the constant-$\dot{\alpha}$ dynamic-stall phenomena. Francis et al. did not perform a systematic study of constant-$\dot{\alpha}$ motions; however, a number of specific cases were run for $\dot{\alpha}_{ND}$ of approximately 0.05–0.15. Although the rotation points were for $x/c=0.31$ and 0.375 rather than 0.5 (as in the present study) and the $\dot{\alpha}_{ND}$ range did not overlap the present study, a number of observations were made that were similar to those made here. For one, Ref. 15 noted a "notch" in the $C_L-\alpha$ curves, which we believe to be equivalent to what we describe as a plateau. Also, the qualitative character of $C_D$ and $C_M$ curves appear to be in general agreement with the present findings. Although the $\dot{\alpha}_{ND}$ of Ref. 15 were as much as three times those of the present work, the $(C_L)_{MAX}$ reported in REf. 15 do not appear to be correspondingly larger than those we observed.

Walker et al.[16] also show similar qualitative features to those of the present work. Reference 16 reports on data for equivalent $\dot{\alpha}_{ND}$ of approximately 0.025–0.3 and a $(C_L)_{MAX}$ as high as 4.0 was reported for an $\dot{\alpha}_{ND}$ equivalent of 0.3. In this regard, the Ref. 16 $(C_L)_{MAX}$ results are in agreement with those we would expect and are not consistent with those of Ref. 15. It should also be noted that, while Ref. 16 reports an effect of $C_L-\alpha$ slope on $\dot{\alpha}_{ND}$, it appears to be in contradiction to that of the present work in some, although not all, instances.

## Conclusions

This paper has reported on a systematic study of the dynamic-stall event for a constant-$\dot{\alpha}$ pitching airfoil. Because of the simplicity of the experimental design, we believe that the results reported on here provide insight into the mechanisms at work in the dynamic-stall process. We use the word process to emphasize that different mechanisms are at work at different points in the dynamic-stall event. It is clear that the delay in quarter-chord separation plays a key role in dynamic stall and, as such, it is important to understand the physics causing this delay. In this regard, the subtleties suggested to be present in the attached flow region indicate that the external flow model of Ref. 7 could be helpful in further boundary-layer studies.

Finally, it seems appropriate to close by addressing three major questions that should be asked concerning the dynamic-stall phenomena; these are how large are the effects, are these effects reproducible enough to be exploited, and finally, if sufficiently reproducible to be exploited, where are the possible payoffs? This paper answers the first two questions; the effects are large [perturbations in motion of less than 3% more than doubling the $(C_L)_{MAX}$] and the reproducibility is clearly present in the data, even down to preserving small detail in both the prestall and poststall region.

With regard to the third question, that of exploitation and payoff, this must wait for future studies. However, it is of some note that the character of the drag and moment curves suggest a manageable behavior from a stability-and-control point of view. The drag, for example, remains low far into the region beyond static stall and the moment is of the pitch-down type, which would aid in regaining attached-flow angles of attack.

## References

[1]Kramer, von M., "Die Zunahume des Maximalauftriesbes von Tragflügeln bei plotzlicher Anstellwinkelvergrö Berung (Böeneffekt)," *Zietschrift für Flugtechnik und Motorluftschiffahrt,* Vol. 7, April 14, 1932, pp. 185–189.

[2]Ericsson, L.E. and Reding, J.P., "Unsteady Airfoil Stall, Review and Extension," *Journal of Aircraft,* Vol. 8, Aug. 1971, pp. 609–616.

[3]Ericsson, L.E., and Reding, J.P., "Unsteady Flow Concepts for Dynamic Stall Analysis," *Journal of Aircraft,* Vol. 21, Aug. 1984, pp. 601–606.

[4]Daley, D.C. and Jumper, E.J., "Experimental Investigation of Dynamic Stall for a Pitching Airfoil," *Journal of Aircraft,* Vol. 21, Oct. 1984, pp. 831–832.

[5]Jumper, E.J., "Mass Ingestion: A Perturbation Method Useful in Analyzing Some Boundary-Layer Problems," ASME Paper 86-WA/FE-10, Dec. 1986.

[6]Jumper, E.J., Hitchcock, J.E., Lawrence, T.S., and Docken, R.G. Jr., "Investigating Dynamic Stall Using a Modified Momentum-Integral Method," AIAA Paper 87-0431, Jan. 1987.

[7]Tupper, K.W., "The Effect of Trailing Vortices on the Production of Lift on an Airfoil Undergoing a Constant Rate of Change of Angle of Attack," Thesis, Air Force Institute of Technology, Wright-Patterson AFB, OH, Rept. AFIT/GAE/AA/83D-24, Dec. 1983.

[8]Allaire, A.J.S., "Investigation of Potential and Viscous Flow Effects Contributing to Dynamic Stall," Thesis, Air Force Institute of Technology, Wright-Patterson AFB, OH, Rept. AFIT/GAE/AA/84S-1, Sept. 1984.

[9]Schreck, S.J., "Continued Experimental Investigation of Dynamic Stall," Thesis, Air Force Institute of Technology, Wright-Patterson AFB, OH, Rept. AFIT/GAE/AA/83D-21, Dec. 1983.

[10]Dimmick, R.L., "Pitch-Location Effects on Dynamic Stall," Thesis, Air Force Institute of Technology, Wright-Patterson AFB, OH, Rept. AFIT/GAE/AA/85D-4, Dec. 1985.

[11]McAlister, K.W., Carr, L.W., and McCroskey, W.J., "Dynamic Stall Experiments on the NACA 0012 Airfoil," NASA TP 1100, 1978.

[12]Jumper, E.J., Schreck, S.J., and Dimmick, R.L., "Lift-Curve Characteristics for an Airfoil Pitching at Constant Rate," AIAA Paper 86-0117, Jan. 1986.

[13]Walker, J.M., Helin, H.E., and Strickland, J.H., "An Experimental Investigation of an Airfoil Undergoing Large Amplitude Pitching Motions," AIAA Paper 85-0039, Jan. 1985.

[14]Chow, C.Y. and Chiu, C.S., "Unsteady Loading on an Airfoil Due to Vortices Released Intermittently from its Surface," *Journal of Aircraft,* Vol. 23, Oct. 1986, pp. 750–755.

[15]Francis, M.S., Keesee, J.E., and Retelle, J.P. Jr., "An Investigation of Airfoil Dynamic Stall with Large Amplitude Motion," F.J. Seiler Research Laboratory, U.S. Air Force Academy, CO, Rept. FJSRL-TR183-0010, Oct. 1983.

[16]Walker, J., Helin, H. and Chou, D., "Unsteady Surface Pressure Measurements on a Pitching Airfoil," AIAA Paper 85-0532, March 1985.